A Modular Multilevel Converter with DHB Energy Balancing Channels for Medium-Voltage Adjustable-Speed Drives

Mohamed S. Diab*, Derrick Holliday*, A. M. Massoud†, Shehab Ahmed‡, B. W. Williams*

*Electronic and Electrical Engineering Dept., University of Strathclyde, Glasgow, U.K.,
†Electrical Engineering Dept., Qatar University, Doha, Qatar,
‡Electrical and Computer Engineering Dept., Texas A&M University at Qatar, Doha, Qatar

Keywords: Dual half-bridge (DHB), medium-voltage variable-speed drives, modular multilevel converter (MMC), power decoupling, submodule (SM) capacitor voltage-ripple.

Abstract

This paper presents a modular multilevel converter (MMC) configuration that utilises energy exchange between submodules (SMs) of upper and lower arms, for energy rebalancing. The configuration is applicable to medium-voltage high-power variable-speed drives with any number of motor phases, where the traditional MMC topology experiences challenging shortcomings. With the out-of-phase alternation of the fundamental ripple power in upper and lower arms, the proposed MMC configuration decouples this ripple power by employing dual half-bridge modules linking opposite SMs in upper and lower arms of the same MMC-leg. This counter-balances arm ripple-power through bidirectional power transfer between opposite SMs, resulting in a reduction in the SM capacitance and the MMC system stored energy. The proposed MMC configuration solves the problem of wide SM capacitor voltage fluctuation, especially at low operating frequencies, where the SM capacitor voltage ripple profile is almost constant, independent of the operating frequency. Therefore, the configuration is able to drive multi-megawatt machines from stand-still to the rated speed, at rated torque. The operation of the proposed converter topology is elucidated in detail, and its effectiveness is verified through simulation and experimentation.

1 Introduction

With its superior features, the modular multilevel converter (MMC) is considered a competitor for high-voltage high-power applications, outperforming its counterparts [1]. Being in the multilevel category, the MMC inherits the advantages of the state-of-the-art multilevel converter topologies [2]-[4], while solely enjoying the features of modularity, scalability, redundancy, and reliability [5]. These advantages promoted the MMC to be adopted in industry as a commercialized converter interface in high-voltage direct-current transmission systems [6]. In addition, the crucial need for high-power drives at medium-voltage (MV) level shows favour for the MMC to be the next generation motor-drive technology.

Due to its unique operating principles, the MMC performance is highly depending on the operating frequency, where pulsating ripple power at both the fundamental and second-order harmonic are experienced by the MMC arms. This ripple power is eventually manifested in the MMC submodule (SM) capacitor in a voltage ripple profile that has the first and second harmonics as the most dominant components. Both capacitor voltage ripple components were found to be in an inverse proportion to the operating frequency. That is why MMC application in the MV adjustable-speed drives market is still bounded, unless for a narrow range of quadratic-torque loads such as fans, pumps, and compressors [7], [8].

Through extensive developing efforts, the MMC has been addressed in the literature for MV adjustable-speed drives application. Two main approaches have been adopted to restrain the capacitor voltage ripple challenge; software solutions that propose new modulation and control methods [9], [10], and hardware ones that suggest structural changes in the traditional MMC topology [11], [12]. Although most of the introduced solutions satisfactorily suppress SM capacitor voltage-ripple at low operating frequencies, they are unable to drive a machine at full-load torque from a stand-still condition, rendering the need for a comprehensive solution still triggered.

The authors have recently proposed a new approach for MMC ripple-power decoupling, which overcomes the SM capacitor voltage ripple problem. The approach is based on employing chains of dual half-bridge (DHB) modules between MMC SMs, acting as energy balancers at the SM level. The power decoupling approach has been applied to three-phase machines with both open-end stator windings [13] and star and delta connections [14], in addition to symmetrical six-phase machines [15]. In these three applications, the power decoupling is implemented in a horizontal scheme, where the excess of the capacitive energy at each SM is transferred to the adjacent-arm SM in another phase-leg, to cater for the lack of energy. In this paper, the concept of the power decoupling is generalized for any type of machine with any number of phases, where the power is decoupled in a vertical scheme between SMs in the upper and lower arms of the same phase-leg. MMC arm ripple power decoupling results in a significant reduction in SM capacitance in addition to a bounded SM capacitor voltage ripple.

In the next two sections, the pulsating ripple power problem and its effects on the SM capacitor voltage ripple are briefly discussed, then the proposed solution is presented.

2 Ripple Characterization of Conventional MMC

A circuit diagram for one MMC phase-leg is shown in Figure 1, where it is formed by two series arms connected through arm inductors L_{arm}, while each arm consists of N series-connected SMs. The SM is commonly a half-bridge (HB) cell employing a dc capacitor of an equivalent capacitance C and a rated voltage V_c, acting as an energy buffer. The output voltage and load current for a general phase-leg j are denoted by v_{jo} and i_j, respectively, and expressed as:

$$\begin{cases} v_{jo} = V_o \cos(\omega t + \theta_j) \\ i_j = I_o \cos(\omega t + \theta_j - \emptyset) \end{cases} \quad (1)$$

where V_o and I_o are the voltage and current amplitudes, respectively, ω is the output angular frequency, θ_j is the phase angle of the output voltage, which depends on the number of the MMC phase-legs, and $\emptyset$ is the load angle. The magnitude of the ac output voltage is defined by the modulation index M and the voltage of the input source V_{dc}, as follows.

$$V_o = \frac{1}{2} M V_{dc} \quad (2)$$

The MMC arm voltages in addition to the arm currents are given by (3) and (4), respectively, with the subscripts U and L denoting the corresponding 'upper' and 'lower' arm.

$$\begin{cases} v_{Uj} = \frac{1}{2} V_{dc} - v_{jo} \\ v_{Lj} = \frac{1}{2} V_{dc} + v_{jo} \end{cases} \quad (3)$$

$$\begin{cases} i_{Uj} = i_{cm\,j} + \frac{1}{2} i_j \\ i_{Lj} = i_{cm\,j} - \frac{1}{2} i_j \end{cases} \quad (4)$$

where $i_{cm\,j}$ is the common-mode (CM) current of the phase-leg j, which can be considered as a dc component assuming the even-order harmonics are suppressed with an appropriate control method [16]. With a lossless input-output power balance for the MMC phase-leg j, the CM current is generally defined as:

$$i_{cm\,j} = \frac{I_{dc}}{m} = \frac{3 M I_o \cos \emptyset}{4m} \quad (5)$$

where I_{dc} is the dc input current, while m is the number of the MMC phase-legs. To simplify the analysis, m will be set to 3 (that is, a three-phase MMC system).
To quantify the ripple components in the SM capacitor voltage, the pulsating ripple power in MMC arms is first calculated as:

$$\begin{cases} p_{Uj} = v_{Uj}\, i_{Uj} \\ p_{Lj} = v_{Lj}\, i_{Lj} \end{cases} \quad (6)$$

Substituting (1)−(5) into (6) and rearranging terms yields,

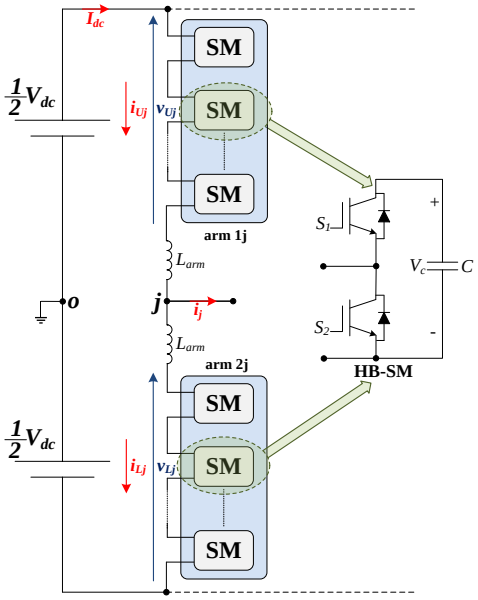

Figure 1: Circuit diagram of an MMC phase-leg using HB-SMs.

$$\begin{cases} p_{Uj} = p_{cm} + p_{dm} \\ p_{Lj} = p_{cm} - p_{dm} \end{cases} \quad (7)$$

$$p_{cm} = -\frac{V_{dc}\, I_o M}{8} \cos[2(\omega t + \theta_j) - \emptyset] \quad (8a)$$

$$p_{dm} = \frac{V_{dc}\, I_o}{8} \sqrt{4 + \cos^2(\emptyset)(M^4 - 4M^2)}\, \cos(\omega t + \theta_j - \gamma) \quad (8b)$$

where p_{cm} and p_{dm} are the CM and differential-mode (DM) components of the arm power, respectively, while γ is a phase-shift angle defined as:

$$\gamma = \emptyset + \tan^{-1} \frac{M^2 \tan \emptyset \cos^2 \emptyset}{2 - M^2 \cos^2 \emptyset} \quad (9)$$

The arm ripple-power expressions show that the DM component pulsates with the fundamental frequency and appears in antiphase in the upper and lower arms as a consequence of the load current being split differentially between them. Whereas, the CM component pulsates at twice the fundamental frequency due to the different frequency alternation of both input and output powers.
Due to the dual frequency alternation of the MMC arm powers, capacitor voltage-fluctuations have both CM and DM voltage-ripple components alternating at twice the fundamental frequency and at the fundamental frequency, respectively, as demonstrated by (10).

$$\Delta v_{c_{Uj}} = -\frac{\Delta V_{c\,cm}}{2} \sin[2(\omega t + \theta_j) - \emptyset] + \frac{\Delta V_{c\,dm}}{2} \sin(\omega t + \theta_j - \gamma) \quad (10a)$$

$$\Delta v_{c_{Lj}} = -\frac{\Delta V_{c\,cm}}{2} \sin[2(\omega t + \theta_j) - \emptyset] - \frac{\Delta V_{c\,dm}}{2} \sin(\omega t + \theta_j - \gamma) \quad (10b)$$

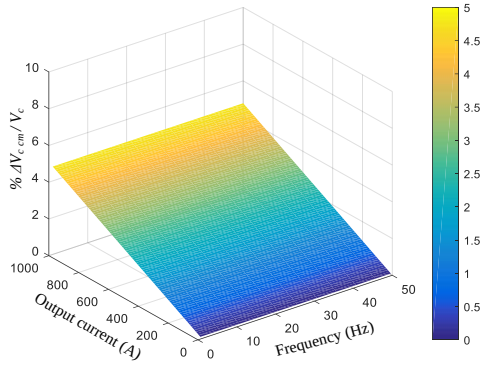

(a)

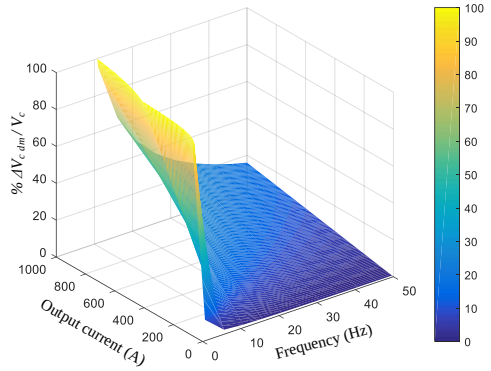

(b)

Figure 2: Relationship of capacitor voltage-ripple at constant M/ω with operating frequency and output current. (C = 3 mF, V_c = 2.5 kV, and $\emptyset$ = 35^0) (a) CM component. (b) DM component).

where Δv_c and ΔV_c are the capacitor voltage-variation and the absolute peak-to-peak variation of the SM capacitor voltage-ripple, respectively. The magnitude of the peak-to-peak capacitor voltage-ripple due to CM and DM components are [13]:

$$\Delta V_{c\,cm} = \frac{I_o M}{8\omega C} \tag{11a}$$

$$\Delta V_{c\,dm} = \frac{I_o}{4\omega C}\sqrt{4+\cos^2(\emptyset)(M^4-4M^2)} \tag{11b}$$

Figure 2 shows the 3-D curves of normalized capacitor voltage ripple duo to both CM and DM components, varied with both operating frequency and output current, while the ratio M/ω is set constant as a requirement of constant motor torque condition. Figure 2a elucidates that the CM component has a slight effect on capacitor voltage-ripple, only with load current increase, where for a 1000 A current increase, the CM voltage ripple constitutes ±2.5%, independent of the operating frequency. In contrast, Figure 2b shows the DM component has a dominant influence on SM capacitor voltage-ripple as it significantly increases with both operating frequency reduction and output current increase.

3 Proposed MMC-DHB Configuration

As established in the previous section, the DM ripple power is a dominant component which is eventually the major contributor to SM capacitor voltage ripple. The amount of the DM ripple power released by an MMC arm and that absorbed by the complementary arm in the same MMC phase-leg, are equal. Therefore, a modular scheme of decoupling the DM ripple power in both the upper and lower arms of each MMC leg is to divert the excessive energy stored in an upper-arm SM capacitor into a lower-arm one in a closed magnetic loop to compensate its lack of the capacitive energy. This can be realized by linking each pair of upper- and lower-arm SM, in the same phase-leg, with magnetic chains of DHB modules allowing the ripple power to be transferred in both directions. This is schematically illustrated in Figure 3 for one MMC phase-leg, where the upper and lower arms are lateral to each other to better visualize the DHB chains. A circuit diagram for a DHB chain link is shown in Figure 4. The DHB converter is composed of a pair of voltage-fed HB inverters interfaced through a high-frequency (HF) transformer [17]. The transformer turns ratio is unity since the dc-dc conversion is only employed for energy equalization between bridge sides at the same voltage level. DHB parasitic components are exploited to achieve some operational characteristics, where the leakage inductance of the HF transformer is employed as an energy transfer element between dc capacitors, while the output capacitance of switching devices is used to realize soft-switching operation. The DHB topology is realised with the MMC SM capacitor equally split, to provide a centre-tap node.

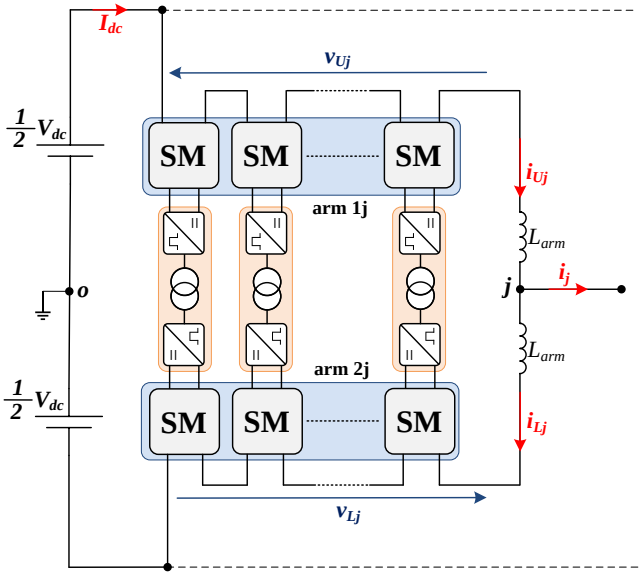

Figure 3: Circuit diagram for the proposed MMC configuration for one phase-leg.

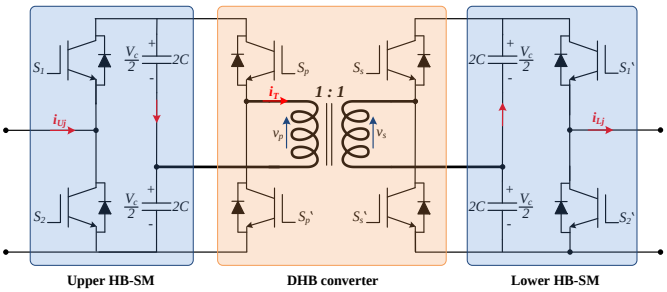

Figure 4: DHB configuration linking two HB-SMs of upper and lower MMC arms.

The decoupling of the DM power component ultimately compensates the DM capacitor voltage ripple. Whereas, the CM power component remains unchanged in both upper and lower arms, since both the releasing and absorption action of such component occurs simultaneously in both arms. Therefore, the CM voltage ripple component is the only one affecting the SM capacitor voltage, as follows.

$$\Delta v_{c_{Uj\ proposed}} = \Delta v_{c_{Lj\ proposed}} = -\frac{I_o M}{16\omega C} sin\left[2(\omega t + \theta_j) - \emptyset\right] \quad (12)$$

$$\Delta V_{c\ proposed} = \Delta V_{c\ cm} = \frac{I_o M}{8\omega C} \quad (13)$$

3.1 DHB Principles of Operation

Since the DHB circuit creates two square-wave voltages on each side of the transformer, the power flow is controlled via the phase angle difference, δ, between the primary and secondary voltage vectors. The most common approach for square-wave generation at both converter side is the phase-shift PWM in which each converter side is modulated with a triangular carrier signal of a frequency ω_h and a constant duty ratio of 50% ($D = 0.5$). Depending on the phase angle difference between the primary and secondary voltages, the power transfer can be calculated to be [13]:

$$P = \frac{{V_c}^2 \sigma(\pi - |\sigma|)}{8\pi^2 f_h L} \quad (14)$$

where L is the transformer leakage inductance and f_h is the DHB switching frequency.
To generate a phase difference δ between DHB converter sides, two modulation signals are defined as follows [18]:

$$M_1 = D - \frac{\delta}{\pi} \quad (15a)$$

$$M_2 = |1 - M_1| \quad (15b)$$

According to the sign of δ, the power transferred between both DHB converter sides can be reversed, as illustrated in Figure 5, where v_p and v_s are the voltages applied on the primary and secondary transformer sides, respectively.

3.2 DHB Control

DHB module control is ultimately to track both the level and direction of power exchange between opposite MMC SMs, which rebalances the stored capacitive energy among the SMs. To compensate the fundamental voltage ripple component, a simple control loop employing a PI controller is implemented for each DHB module. The capacitor voltage ripple at each DHB side is set to zero, while the actual SM voltage ripple is obtained from the capacitor voltage via a high-pass filter. The PI controller provides a reference phase-shift angle, δ^*, to control the power flow between both sides of the DHB, which is utilized in the DHB modulation to generate the DHB switching signals.

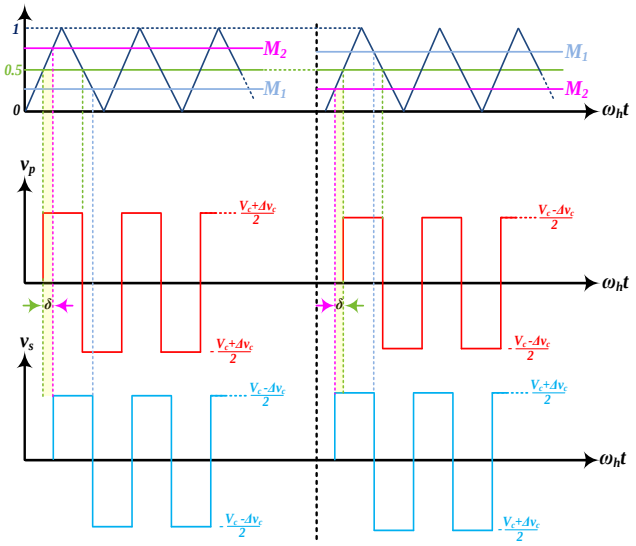

(a) (b)

Figure 5: Sketch map of the phase-shift PWM of DHB converter for bidirectional power transfer. (a) Positive phase-shift angle and (b) Negative phase-shift angle.

Parameter	Simulation	Experiment
Number of SMs per arm (N)	10	3
Input dc voltage (V_{dc})	20 kV	300 V
Nominal SM capacitor voltage (V_c)	2 kV	100 V
Rated active power	10 MW	3 kW
Rated current magnitude (I_o)	700 A	15 A
Fundamental output frequency (f_o)	50 Hz	50 Hz
Carrier frequency of MMC (f_c)	2 kHz	2 kHz
Switching frequency of DHB (f_h)	10 kHz	10 kHz
Load	Induction motor 12 kV, 600 rpm 10 poles	RL load R=10×$\frac{f_o}{50}$ Ω L=12 mH
Arm inductance (L_{arm})	2 mH	2.8 mH
Equivalent SM capacitance (C)	2 mF	1.1 mF

Table 1: Parameters for simulation and experimental studies.

4 Verification

The effectiveness of the proposed MMC-DHB configuration has been examined through simulation in addition to experimentation, with the parameters listed in Table 1.

4.1 Simulation Results

A three-phase MMC-DHB system model is built using MATLAB/SIMULINK, and used to drive a 10 MW 12 kV induction motor from stand-still to the rated speed. The MMC performance during start-up is depicted in the results of Figure 6. The three-phase motor currents show high-quality sinusoidal waveform within the entire speed range. Also, the arm currents of phase a exhibit an out-of-phase profile with even-order harmonics. The voltage ripple of both the upper- and lower-arm SM capacitors pulsate at

twice the fundamental frequency due to the CM ripple component, and is bounded within ±5% over the whole speed range. Although the motor currents are near dc at zero motor speed, the capacitor voltage ripple is totally controllable. The dc input current is continuous with only switching harmonics, while the CM voltage at the motor terminals is limited to ±1.3 kV.

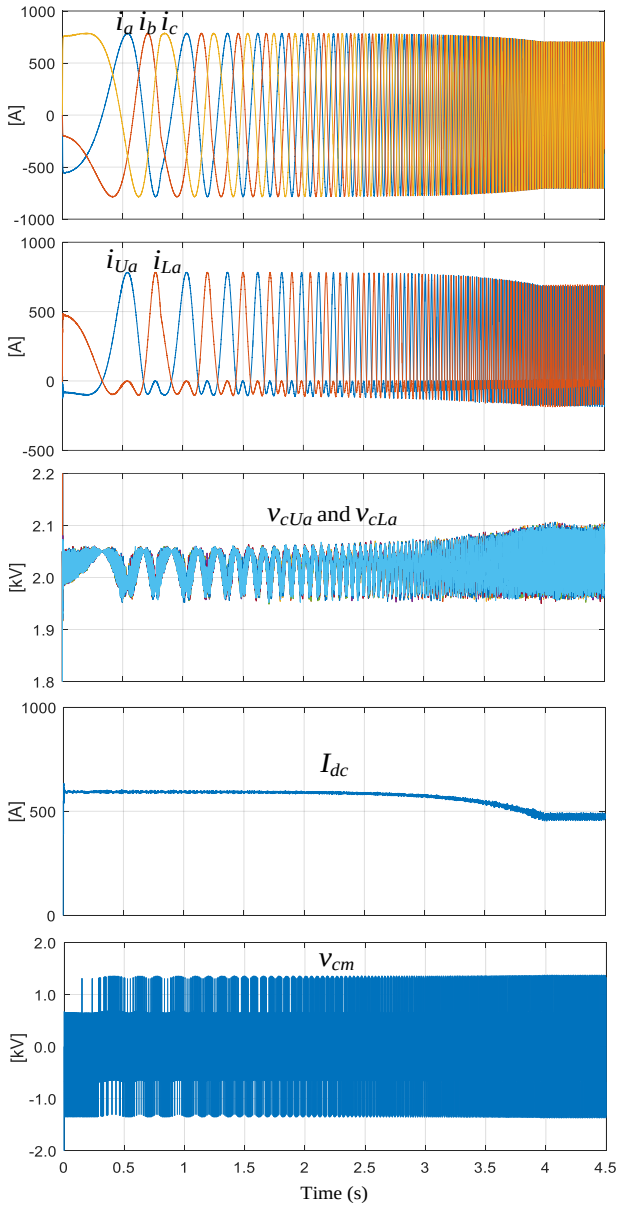

Figure 6: Simulation results for the performance of the proposed MMC system driving a 10 MW induction machine from standstill to the rated speed.

4.2 Experimental Results

A 3 kW laboratory prototype is used to experimentally verify the features of the proposed configuration at different operating frequencies. The prototype employs a three-phase MMC, with 3 SMs per arm, fed from a 300 V dc-link. The experimental results are presented in Figures 7-9. The line voltages and load currents are shown in Figure 7 when the MMC is feeding three-phase *RL* load at the rated parameters of Table 1. Figure 8 shows the switching waveforms of the DHB balancing module including the voltage at both the primary- and secondary-side of the HF transformer, in addition to the transformer current. Figure 9 exhibits the significant influence of the DHB modules incorporation in the proposed MMC configuration, showing the SM capacitor voltage-ripple before and after DHB activation at different operating frequencies. In this case, the output voltage is reduced in accordance to the operating frequency reduction, while the load resistance is varied linearly with the operating frequency to maintain the output current constant at the rated value, at all frequencies, to emulate the constant torque characteristic of variable-speed motors. It should be noted that Figure 9 shows a vertical zoom of the capacitor voltage ripple, where the average SM capacitor voltage is 100 V. From left to right, the capacitor voltage-ripple is shown with the DHB modules deactivated and operational, respectively, where the percentage reduction in the SM capacitor voltage-ripple, due to the activation of DHB modules, is recorded as 42%, 52%, 66%, and 84% at 50 Hz, 10 Hz, 5 Hz, and 1 Hz, respectively.

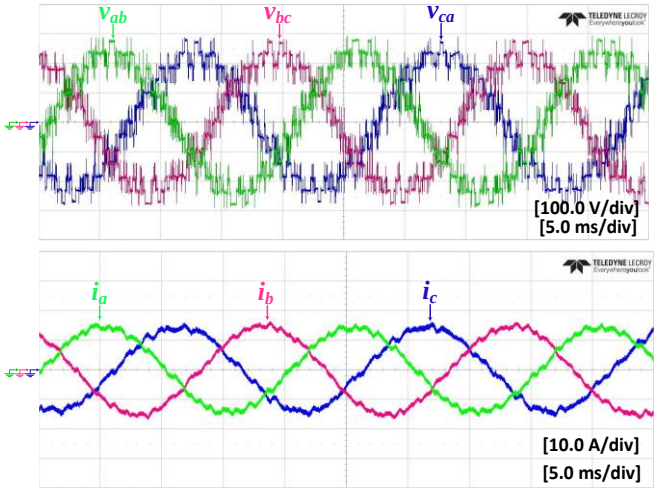

Figure 7: Experimental waveforms for the line voltages and load currents of the proposed MMC at 50 Hz.

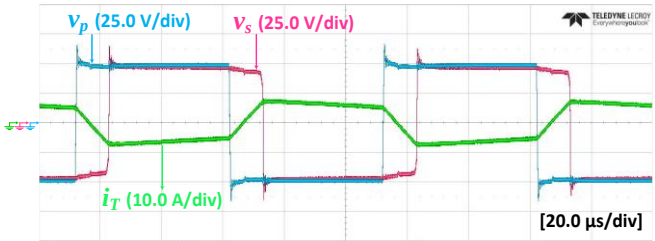

Figure 8: Switching waveforms of the DHB at 10 kHz.

5 Conclusion

This paper extended a previously proposed ripple power decoupling approach for MMC-fed adjustable-speed drives by introducing a new placement scheme for the power decoupling channels. The resulting configuration is suitable

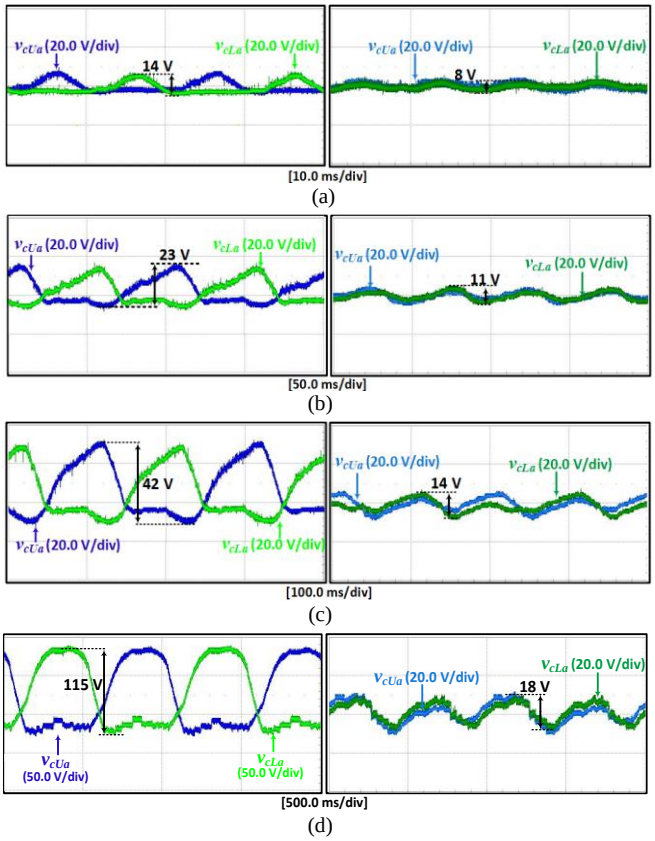

Figure 9: SM capacitor voltage-ripple with DHB modules deactivated (left) and activated (right) at (a) 50 Hz, (b) 10 Hz, (c) 5 Hz, and (d) 1 Hz.

for MV machine drives incorporating any number of motor phases, independent of the machine winding connection. The configuration is characterized by the insertion of magnetic chains equipped with DHB modules linking each pair of upper and lower SMs with the same MMC phase-leg. Since the fundamental ripple-power of opposite SMs of the upper and lower arms alternates with an opposite phase, the DHB modules can decouple this fundamental ripple-power, allowing the capacitive stored-energy to be evenly distributed among all SMs. Therefore, the proposed configuration offers a significant reduction in the SM capacitance since the voltage fluctuations across the capacitors are reduced to a narrow band, which also reduces the energy stored in the converter system. Further, it eliminates the problem of capacitor-voltage fluctuations in an independent operating frequency scheme. The proposed configuration guarantees continuous operation of adjustable-speed drives at any speed/torque condition, with the ability of driving multi-megawatt machines from stand-still at full-load torque.

References

[1] S. Debnath, J. Qin, B. Bahrani, M. Saeedifard, and P. Barbosa, "Operation, control, and applications of the modular multilevel converter: A review," *IEEE Trans. Power Electron.*, vol. 30, no. 1, pp. 37–53, Jan. 2015.

[2] A. Bendre, G. Venkataramanan, D. Rosene, and V. Srinivasan, "Modeling and design of a neutral-point voltage regulator for a three-level diode clamped inverter using multiple-carrier modulation," *IEEE Trans. Ind. Electron.*, vol. 53, no. 3, pp. 718–726, Jun. 2006.

[3] I.-D. Kim, E.-C. Nho, H.-G. Kim, and J. S. Ko, "A generalized Undeland snubber for flying capacitor multilevel inverter and converter," *IEEE Trans. Ind. Electron.*, vol. 51, no. 6, pp. 1290–1296, Dec. 2004.

[4] S. Sirisukprasert, J. S. Lai, and T. H. Liu, "Novel cascaded multilevel converter drive system with minimum number of separated DC sources," in Proc. *IEEE PESC*, Vancouver, BC, Canada, Jun. 17–22, 2001, pp. 1346–1350.

[5] A. Lesnicar and R. Marquardt, "An innovative modular multilevel converter topology suitable for a wide power range," in *Proc. IEEE Power Tech. Conf.*, Bologna, Italy, Jun. 23–26, 2003, vol. 3.

[6] J. Dorn, H. Gambach, J. Strauss, T. Westerweller, and J. Alligan, "Trans bay cable–a breakthrough of vsc multilevel converters in hvdc transmission," in *Cigre Colloquium*, 2012.

[7] A. Korn, M. Winkelnkemper, and P. Steimer, "Low output frequency operation of the modular multi-level converter", in *Proc. IEEE ECCE*, 2010, pp. 3993–3997.

[8] S. Debnath, J. Qin and M. Saeedifard, "Control and Stability Analysis of Modular Multilevel Converter Under Low-Frequency Operation," *IEEE Trans. Ind. Electron*, vol. 62, no. 9, pp. 5329-5339, Sept. 2015.

[9] A. Antonopoulos, L. Ängquist, H. P. Nee, "Optimal Selection of the Average Capacitor Voltage for Variable-Speed Drives with Modular Multilevel Converters," *IEEE Trans. Power Electron.*, vol. 30, no. 1, pp. 227-234, Jan. 2015.

[10] B. Tai; C. Gao; X. Liu; Z. Chen, "A Novel Flexible Capacitor Voltage Control Strategy for Variable-Speed Drives with Modular Multilevel Converters," *IEEE Trans. Power Electron.*, vol. 32, no. 1, pp. 128-141, Jan. 2017.

[11] S. Du; B. Wu; N. Zargari; Z. Cheng, "A Flying-Capacitor Modular Multilevel Converter (FC-MMC) for Medium-Voltage Motor Drive," *IEEE Trans. Power Electron*., vol. 32, no. 3, pp. 2081-2089, March 2017.

[12] Z. Kong; X. Huang; Z. Wang; J. Xiong; K. Zhang, "Active Power Decoupling for Submodules of Modular Multilevel Converter," *IEEE Trans. Power Electron*, vol. PP, no.99, pp.1-1.

[13] M. S. Diab; A. M. Massoud; S. Ahmed; B. W. Williams, "A Dual Modular Multilevel Converter with High-Frequency Magnetic Links Between Sub Modules for MV Open-End Stator Winding Machine Drives," *IEEE Trans. Power Electron*., vol. PP, no.99, pp.1-1.

[14] M. S. Diab; A. M. Massoud; S. Ahmed; B. W. Williams, "A Modular Multilevel Converter with Ripple-Power Decoupling Channels for Three-Phase MV Adjustable-Speed Drives," *IEEE Trans. Power Electron*., vol. PP, no.99, pp.1-1.

[15] M. S. Diab, B. W. Williams, D. Holliday, A. M. Massoud and S. Ahmed, "A modular multilevel converter with isolated energy-balancing modules for MV drives incorporating symmetrical six-phase machines," *2017IEEE Energy Conversion Congress and Exposition (ECCE)*, Cincinnati, OH, USA, 2017, pp. 2715-2722.

[16] Z. Li, P. Wang, Z. Chu, H. Zhu, Y. Luo, and Y. Li, "An inner current suppressing method for modular multilevel converters," *IEEE Trans. Power Electron.*, Vol. 28, No. 11, pp. 4873-4879, Nov. 2013.

[17] Hui Li, Fang Zheng Peng and J. S. Lawler, "A natural ZVS medium-power bidirectional DC-DC converter with minimum number of devices," *IEEE Trans. Ind. Appl.*, vol. 39, no. 2, pp. 525-535, Mar/Apr 2003.

[18] A. Zafeiropoulos, A. Antonopoulos and J. R. Svensson, "An MMC-based topology using DHB power channels for load balancing in 50 Hz railway applications," *2017 IEEE Energy Conversion Congress and Exposition (ECCE)*, Cincinnati, OH, 2017, pp. 83-90.